applied sciences

MDPI

Article

Power System Signal-Detection Method Based on the Accelerated Unsaturated Stochastic Resonance Principle

Shuqin Sun [1,2], Xin Qi [1,2], Zhenghai Yuan [1,2], Xiaojun Tang [3,*] and Zaihua Li [3]

[1] College of Instrumentation and Electrical Engineering, Jilin University, Changchun 130061, China; sunsq@jlu.edu.cn (S.S.); xinqi21@mails.jlu.edu.cn (X.Q.); yuanzh22@mails.jlu.edu.cn (Z.Y.)
[2] Key Laboratory of Geophysical Exploration Equipment, Ministry of Education, Jilin University, Changchun 130061, China
[3] China Electric Power Research Institute, Beijing 100192, China; lizaihua@epri.sgcc.com.cn
* Correspondence: tangxiaojun1979@sina.com

Abstract: The classical bistable stochastic resonance algorithm has an inherent output saturation defect that restricts the amplitude of the output signal. This paper examines the causes of this phenomenon and its negative impact on the detection of weak signals. Proposing the Unsaturated Bistable Stochastic Resonance (UBSR) detection algorithm involves constructing a segmented potential function using a linear function to eliminate the effect of higher-order terms in the classical stochastic resonance algorithm. A new type of segmented potential function has been created by combining exponential and linear functions. This new function helps to eliminate the impact of higher-order terms in classical algorithms while also improving the noise immunity of the stochastic resonance system. This results in the development of the accelerated stochastic resonance (ASR) detection algorithm. In this paper, the Kramers escape rate and output signal-to-noise ratio of two improved stochastic resonance algorithms are theoretically derived and compared with the classical bistable stochastic resonance algorithms, and the proposed algorithms are able to effectively avoid the output saturation phenomenon and have more excellent detection performance under strong background noise.

Keywords: stochastic resonance; multistage potential well; correlation number; harmonic detection; voltage dips detection

check for updates

Citation: Sun, S.; Qi, X.; Yuan, Z.; Tang, X.; Li, Z. Power System Signal-Detection Method Based on the Accelerated Unsaturated Stochastic Resonance Principle. *Appl. Sci.* **2024**, *14*, 4284. https://doi.org/10.3390/app14104284

Academic Editor: Andreas Sumper

Received: 12 April 2024
Revised: 15 May 2024
Accepted: 17 May 2024
Published: 18 May 2024

1. Introduction

The power industry is a fundamental sector for the national economy and people's livelihood. Therefore, enhancing the reliability of power supply is one of the crucial tasks of the power industry [1]. In recent years, the widespread use of power electronic technology [2] and the extensive development of new energy generation [3] have led to increasingly serious harmonic pollution in the power system. This pollution has a significant impact on power quality, power system security, and economic operation. At the same time, the power system is not strictly three-phase symmetrical. Even if no faults occur, there will still be harmonics, and the harmonic content will rise sharply during asymmetrical faults. The presence of harmonics can impact power quality, affect the performance of relay protection equipment, increase power grid losses, and affect electronic equipment and precision instruments. To ensure the stable and reliable operation of power systems, high-precision algorithms for detecting power harmonics have become a focus of research. Harmonic management can effectively improve power quality in the power grid [4]. Analyzing the parameters of harmonics to obtain real-time and accurate harmonic data is key to harmonic detection.

Currently, power system harmonic analysis primarily relies on time-domain analysis [5], frequency-domain analysis [6], wavelet transform method [7], and Hilbert–Huang transform method [8]. In classical time-frequency domain analysis methods, spectral overlap occurs when weak power harmonic signals are overwhelmed by a wide spectrum of strong background noise. This makes it difficult to determine the parameters of the filter for extracting weak signals with unknown characteristics.

The literature [5] utilizes the Prony algorithm to analyze power system harmonics and interharmonic signals in the time domain. While the Prony algorithm offers high frequency resolution, this method is easily affected by noise signals and can only accurately estimate the characteristic indexes of harmonic and interharmonic components in the absence of noise or with minimal noise. The detection effectiveness is significantly reduced when weak signals are detected in the presence of strong noise. The frequency domain analysis method has issues such as the window function and the complexity and difficulty of designing the correction method. The study [6] utilizes the improved ap–FFT ratio method for spectral correction, which has a simple correction formula and is easy to implement, but when correcting the amplitude, only the strongest spectral line near the actual frequency point is utilized for the interpolation correction, while the information of the second strongest spectral line is not utilized, and the accuracy of the detection results cannot be guaranteed when the number of sample points does not meet the sufficiently large conditions. The wavelet transform is prone to band aliasing in harmonic decomposition and also has issues such as a large computational workload. The study [7] proposed an improved wavelet transform method but did not address the issue of frequency aliasing, and the harmonic suppression effect is inadequate. The study [8] utilized the Hilbert–Huang transform method, which suffers from modal aliasing and noise sensitivity.

The stochastic resonance algorithm offers several advantages in detecting weak signals. Unlike traditional algorithms, it is not limited by the length of the data set, allowing for the detection of short data sets. Additionally, it considers noise energy as a source of signal energy, resulting in a higher output signal-to-noise ratio. The algorithm is not restricted to a specific signal modulation mode, making it quite versatile. The discussion of stochastic resonance theory in detecting weak feature signals continues to advance due to its unique signal-enhancement capabilities. Leveraging the strengths of the stochastic resonance phenomenon, the successful detection of weak useful signals in a strong background noise environment is a crucial challenge in signal processing. This has significant theoretical importance and wide-ranging practical applications, particularly in the research of new signal-detection methods in power systems.

In our previous research, we found that the combination of a chaotic system with a random resonance detection system can be used to accurately detect the frequency and amplitude of harmonic signals. However, the noise resistance of the chaotic system is generally stronger than that of the random resonance detection system. The chaotic system relies on the random resonance system to detect harmonic frequency when the signal is unknown. Therefore, it is important to improve the noise resistance of the random resonance detection system for detecting harmonic signals in power systems. Additionally, improving the performance of bistable and multistable stochastic resonance detection systems can enhance the detection performance of their single-well approximation models. This breakthrough can enable stochastic resonance to detect non-periodic signals, which is significant for blind detection of other non-periodic signals in power systems under strong background noise.

2. Output Saturation Limits for Classical Stochastic Resonance Models

2.1. Potential Function Model for Bistable Systems

The three necessary conditions for generating stochastic resonance are an input signal, noise, and a bi- or multi-stationary nonlinear system. Therefore, selecting a suitable nonlinear system is important for generating stochastic resonance phenomena.

The bistable system potential function [9] is given by

$$U(x) = -\frac{1}{2}ax^2 + \frac{1}{4}bx^4 \tag{1}$$

where U denotes the potential energy of the bistable system, and x is the characteristic displacement of the bistable system, which is also used as an observation parameter of the system state. a, b are the system parameters of the bistable system, and the potential well image is shown in Figure 1 when the system parameters a, b are varied.

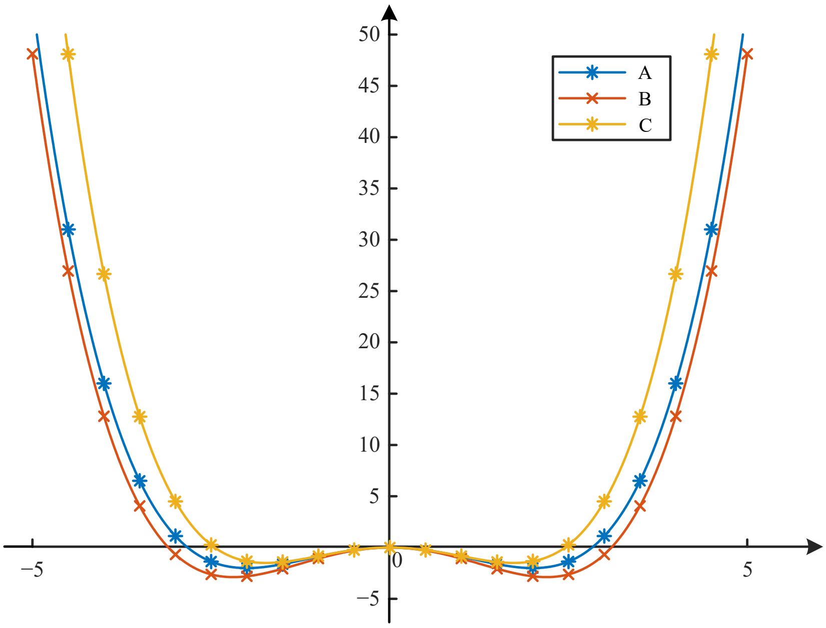

Figure 1. Potential well image of a bistable system.

As can be seen from Figure 1, the potential well height ΔU of the bistable system is related to the parameters a and b with the specific relational expression [10]:

$$\Delta U = \frac{a^2}{4b} \tag{2}$$

Adjusting the values of variables a and b can alter the shape of the potential function, which is crucial in determining whether the particles can successfully make a jump [11]. When comparing the potential function images of group A ($a = 2$, $b = 0.5$) and group B ($a = 2.4$, $b = 0.5$), it is evident that as the system parameter increases, the depth of the potential well deepens and the width of the potential well widens, making it more difficult for particles to make the jump. Similarly, when comparing the potential function images of group A ($a = 2$, $b = 0.5$) and group C ($a = 2$, $b = 2/3$), it is observed that with an increase in the system parameters, the depth of the potential well becomes shallower, the width of the potential well becomes narrower, and it becomes less difficult for the particles to make the leap. In engineering, broad-spectrum background noise is usually modeled as Gaussian white noise $\Gamma(t)$ with a mean value of 0 and an intensity of D:

$$\begin{cases} \langle \Gamma(t) \rangle = 0 \\ \langle \Gamma(t) \cdot \Gamma(t+\tau) \rangle = 2D\delta(\tau) \end{cases} \tag{3}$$

where $\delta(\tau)$ is the unit impulse function, t is time, τ denotes the time between two stochastic processes, and all t and τ appearing later express the same meaning.

When excited only by a periodic signal, the periodic signal affects the potential function of the bistable system, which is expressed as [12]:

$$U(x) = -\frac{1}{2}ax^2 + \frac{1}{4}bx^4 + x[A\cos(\omega_0 t)] \tag{4}$$

The potential curve of the bistable system is periodically tilted at the signal angular frequency ω_0, and the two potential wells periodically rise and fall at the signal angular frequency ω_0 with respect to the base height. At this point, there exists a dual potential well critical amplitude A_C [13]:

$$A_C = \sqrt{\frac{4a^3}{27b}} \tag{5}$$

When $A > A_C$, the system cannot maintain the bistable characteristics; when $A < A_C$, the system still maintains the bistable characteristics, and the signal particles make a periodic motion in only one of the potential wells at the signal frequency ω_0, depending on the initial conditions.

When excited only by random noise $\Gamma(t)$, the signaling particles reciprocally leap between the two potential wells at the Kramers escape rate r_k, which is determined by the noise intensity and the noise probability distribution [14]:

$$r_k = \frac{a}{\sqrt{2}\pi} \exp\left(-\frac{a^2}{bD}\right) \tag{6}$$

When the noise and the periodic signal stimulate the bistable system at the same time, the motion state of the system's potential well and the signaling particle is shown in Figure 2.

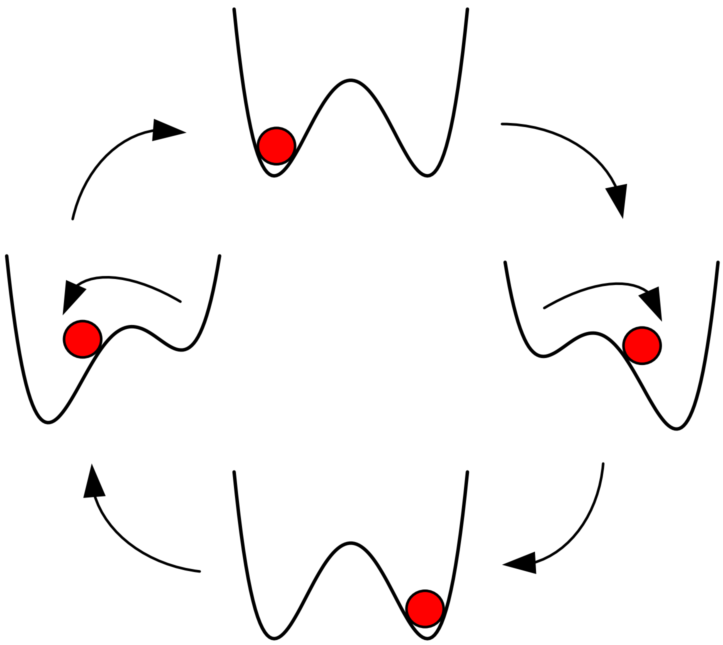

Figure 2. Schematic representation of the system state during mixed signal excitation.

The bistable system is subjected to the joint action of the weak periodic signal and the random noise, and the periodic signal causes the periodic switching of the system's potential wells, which, together with the periodic jumping of the particles caused by the random noise, makes it possible for the particles to reciprocate between the two potential wells in the case of $A < A_C$, and the output of the system (the motion state of the signaling particles) is switched between the two potential wells according to the signal frequency ω_0 (the periodicity of the particle's location switching). When the switching rate ω_0 matches the Kramers escape rate [15], i.e.,

$$r_k = \frac{\omega_0}{\pi} \tag{7}$$

the system's output induced by random noise will have the same frequency as the weak periodic signal. This means that the random noise and the weak periodic signal are output in the form of the same cycle in an orderly manner. This conversion of energy from the noise into the energy of the weak periodic signal augments the weak periodic signal and generates stochastic resonance.

2.2. Output Saturation Limit

Temporarily disregarding the impact of the input signal and input noise on the system, the bistable system's approximate Langevin equation at this juncture is [16]

$$x' = ax - bx^3 \tag{8}$$

Solving this differential equation gives an expression for the amplitude of the output $x(t)$ of the system,

$$|x(t)| = \sqrt{\frac{a}{b + e^{-2at}}} \tag{9}$$

From Equation (9), when the system stabilizes, i.e., at time $t \to \infty$,

$$|x(t)|_{t\to\infty} = \sqrt{\frac{a}{b}} \tag{10}$$

In the adiabatic approximation, the output amplitude of the bistable system is influenced by the system parameters a and b. When the system parameter b = 1, there is a saturation value. Figure 3 shows how the system output amplitude changes with the variation of parameter a while parameter b is fixed at 1. Similarly, Figure 4 illustrates the change in the system output amplitude with the variation of parameter b while parameter a is set to 1.

It is apparent from Figures 3 and 4 that both system parameters "a" and "b" of the bistable system impact the saturation value of the output of the stochastic resonance. However, it is not possible to alter the nature of the saturation of the output, and the output saturation value does not change significantly with the system parameters. Therefore, the performance of the output of the stochastic resonance cannot be significantly improved by changing the system parameters.

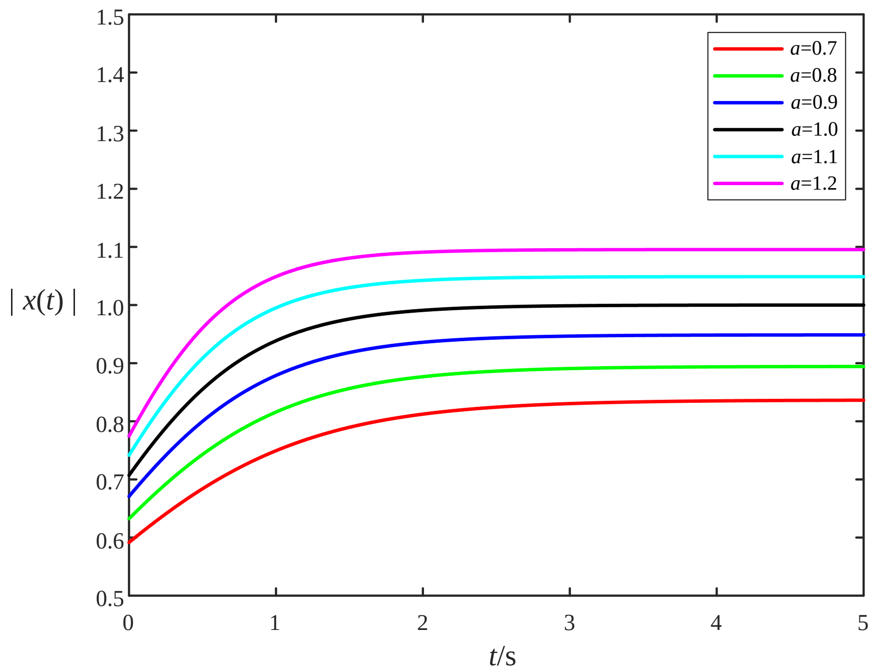

Figure 3. Stochastic resonance output amplitude for different parameter a values.

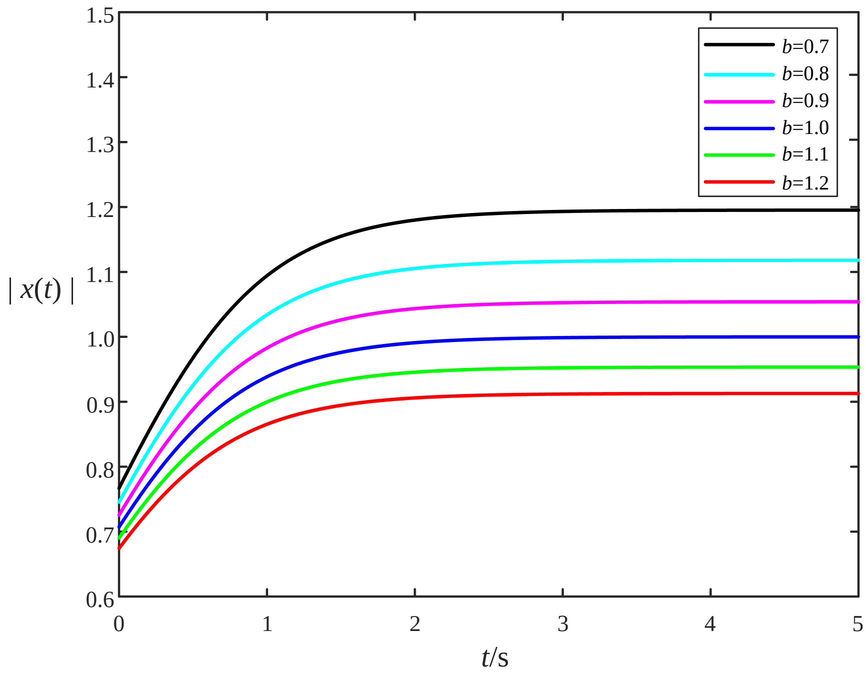

Figure 4. Stochastic resonance output amplitude for different parameter b values.

The output of the stochastic resonance system is equivalent to the displacement trajectory of the equivalent proton. The motion of the equivalent proton is equivalent to the process of converting mechanical energy. To analyze the saturation of the system output, we need to start by examining the system's potential function curve. We analyze the slope of the potential function curve as

$$U^{'}(x) = -ax + bx^3 \tag{11}$$

From Equation (11), it can be observed that the slope of the potential function curve contains cubic terms. This means that the slope of the curve will increase significantly as the displacement increases, as illustrated in Figure 5. After crossing the positive and negative stability points, the displacement increase will result in a substantial increase in potential energy. However, the constraints of the adiabatic approximation conditions cause the input signals and the noise to be of a smaller value, and the energy may not meet the demand of a significant difference in potential energy. As a result, the output of the system will tend to become saturated.

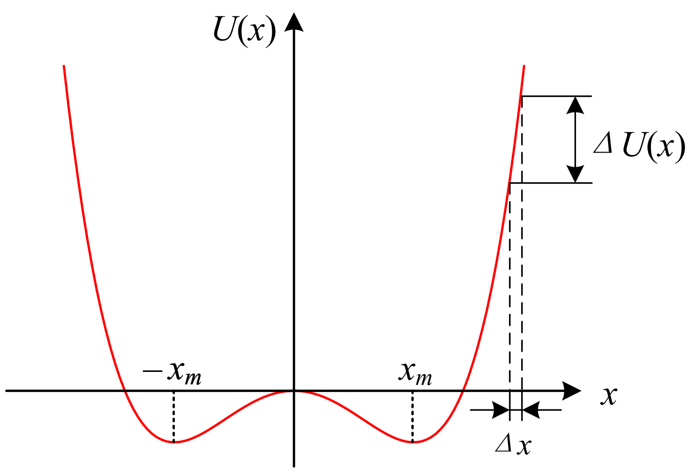

Figure 5. Potential function curve saturation analysis.

From the above analysis, it can be seen that the shape of the system potential well has a significant effect on the output performance of the system, and the different performances of the system can be improved by adjusting the system's potential function.

3. Improved Stochastic Resonance Model with Output Saturation Limits

3.1. Unsaturated Stochastic Resonance Model

After analyzing the potential function of the system, it is evident that the slope of the potential function significantly affects the performance of the stochastic resonance algorithm. The most influential part is the two major potential walls. Therefore, by reducing the slope of the potential wall—that is, lowering the slope of the part of the potential function curve that crosses over the stability—the output performance of the system can be improved.

As shown by the above analysis, the output saturation of the system is mainly affected by the quadratic term x^4 in the potential function; in order to avoid the existence of the quadratic term in the nonlinear potential function, the primary function function is used to construct the Unsaturated Bistable Stochastic Resonance (UBSR) signal detection algorithm, and its potential function is expressed as

$$U_{UBSR} = \begin{cases} -\frac{a^2}{4b}\left(\frac{x+c}{c-\sqrt{a/b}}\right) & x < -\sqrt{\frac{a}{b}} \\ -\frac{1}{2}ax^2 + \frac{1}{4}bx^4 & -\sqrt{\frac{a}{b}} \le x \le \sqrt{\frac{a}{b}} \\ \frac{a^2}{4b}\left(\frac{x-c}{c-\sqrt{a/b}}\right) & x > \sqrt{\frac{a}{b}} \end{cases} \tag{12}$$

The Unsaturated Bistable Stochastic Resonance detection system has a linear and nonlinear two-part system structure, the linear part of the potential barrier wall is treated linearly, and the nonlinear part still retains the original potential function of the bistable system. Since the stochastic resonance phenomenon mainly occurs in the $[-x_m, x_m]$ region [17], the slope of the potential function can be finely tuned to promote the formation of periodic oscillations of the particles between the two potential wells, and the curves of the potential function with different slopes are shown in Figure 6.

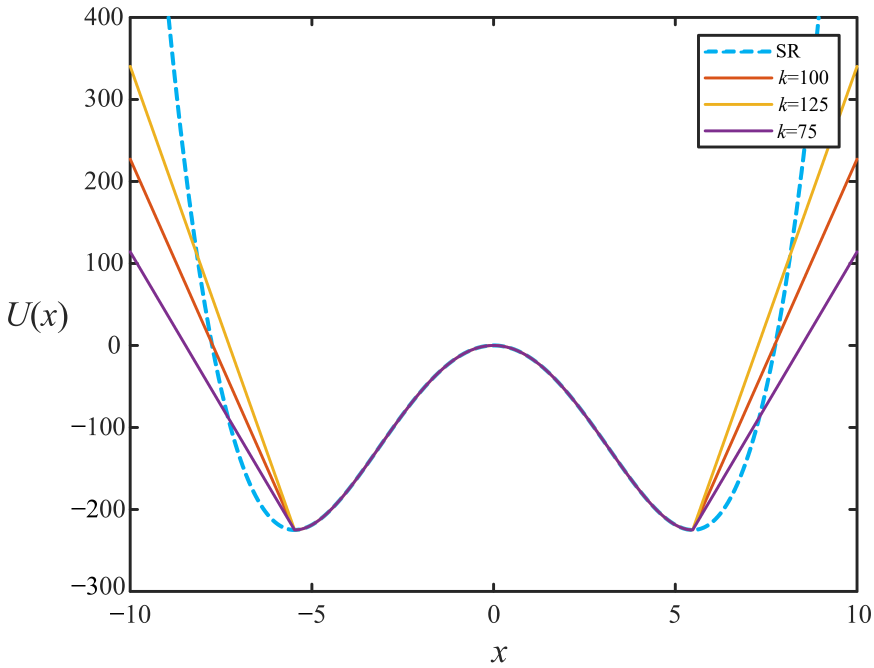

Figure 6. Unsaturated stochastic resonance potential function curves.

As can be seen from Figure 6, the red dashed line is the original dual-potential-well curve, and the rest of the curves are linear potential-well walls with different slopes. By comparison, it is concluded that the linearly improved bistable system can be avoided by changing the slope of the potential-well walls, so that the amplitude of the system's output signal at time $t \to \infty$ no longer tends to a stable saturation value, but rather increases linearly, avoiding the phenomenon of output saturation.

Disregarding the effect of noise, when the signal is input to the system, the system potential function is modulated by the input signal, at which time the potential function is

$$U_s(x) = U(x) - x(A\sin(2\pi f_0 t)) \tag{13}$$

where A is the input periodic signal amplitude, f_0 is the frequency of the input periodic signal, and the setting time is one-quarter cycle and three-quarter cycle, at which time the potential function curve under modulation is shown in Figure 7.

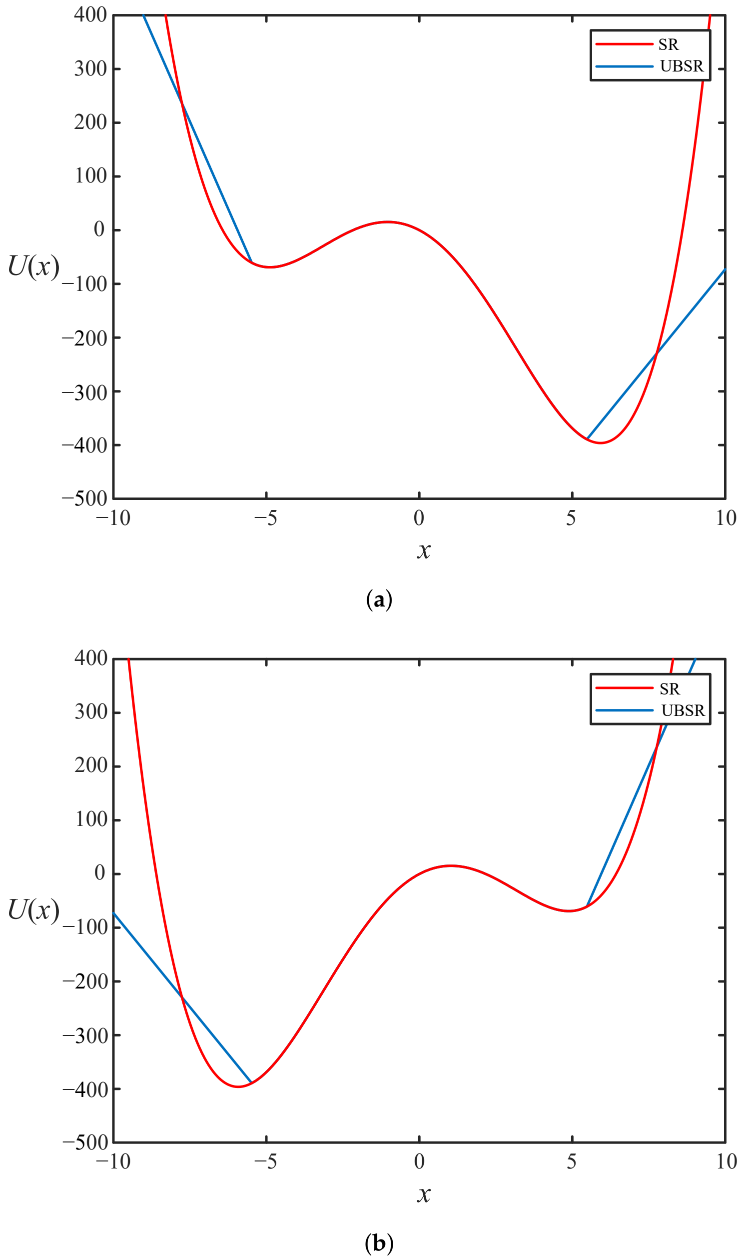

Figure 7. Potential function curves under input signal modulation. (**a**) Potential function curves at quarter-cycle moments. (**b**) Potential function curve at the moment of the three-quarter cycle.

As can be seen in Figure 7, the depth of the left and right potential wells of the potential function of the improved algorithm undergoes alternating transformations, and the period of its dynamic change is consistent with the period of the signal to be detected. When $|x| > \sqrt{a/b}$, the potential function of the improved stochastic resonance signal detection algorithm is always wider than that of the original stochastic resonance signal detection algorithm, indicating that the output signal amplitude can be amplified to a greater extent. Meanwhile, when $\sqrt{a/b} \leq |x| \leq c$, the slope of the outer potential wall increases relative to the average slope of the original potential well, which can promote the oscillation of particles between the two potential wells to some extent.

The Fokker–Planck equation [18] for the Langevin equation corresponding to the non-saturated bistable stochastic resonance algorithm is

$$\frac{\partial\rho(x,t)}{\partial t} = -\frac{\partial}{\partial x}\left[U'\rho(x,t)\right] + D\frac{\partial^2\rho(x,t)}{\partial x^2} \tag{14}$$

where ρ denotes the probability distribution of the particle's location, which is related to the particle's position x and the time t. D is the noise intensity.

The initial probability distribution of the equivalent particle model is assumed to satisfy the adiabatic approximation theory [19]; i.e., it is assumed that the probability distribution at the moment $t = 0$ is concentrated in a certain potential well, i.e., the

$$\rho(x,0) = \delta\left(x \pm \sqrt{\frac{a}{b}}\right) \tag{15}$$

At the same time, it is assumed that the probability flow does not vary with time; i.e., when the

$$\frac{\partial\rho(x,t)}{\partial t} = 0 \tag{16}$$

At the time of integration of Equation (14), the steady-state flow intensity is expressed in terms of Θ, and the stable solution of the Fokker–Planck equation is obtained as

$$U'\rho(x,t) + D\frac{\partial\rho(x,t)}{\partial x} = \Theta \tag{17}$$

Because of the previous assumption that the probability flow does not transform with time at this point, Equation (17) can be rewritten as

$$\frac{d\rho(x)}{\rho(x)} = -\frac{U'(x)}{D}dx \tag{18}$$

to solve Equation (18),

$$\ln\rho(x) = -\frac{1}{D}\int U'(x)dx = -\frac{U(x)}{D} \tag{19}$$

$$\rho(x) = N\exp\left(-\frac{U(x)}{D}\right) \tag{20}$$

where N denotes the constant term to be determined in the stabilized solution in the process of solving the differential equation. Since the object of study in this paper is signal processing and stochastic processes, it is more accurate to say that N denotes the constant process $N(t)$ with respect to the time t. Do not confuse it with $N(f)$ in the simulation part.

From the assumptions of Equation (15), assuming an initial positive potential well, we obtain

$$\delta\left(x - \sqrt{\frac{a}{b}}\right) = N\exp\left(-\frac{U(x)}{D}\right) \tag{21}$$

Integrating Equation (21) yields

$$\int \delta\left(x-\sqrt{\frac{a}{b}}\right)dx = N\int \exp\left(-\frac{U(x)}{D}\right)dx \tag{22}$$

According to the nature of the impulse function, Equation (22) can be simplified to obtain

$$N = \frac{1}{\int \exp\left(-\frac{U(x)}{D}\right)dx} \tag{23}$$

Equation (20) is the chi-square solution of the Fokker–Planck equation, and the following solves for the non-chi-square solution of the Fokker–Planck equation, assuming that

$$\rho(x) = V(x)\exp\left(-\frac{U(x)}{D}\right) \tag{24}$$

follows

$$\frac{d\rho(x)}{dx} = \frac{dV(x)}{dx}\exp\left(-\frac{U(x)}{D}\right) - \frac{U^{'}(x)}{D}V(x)\exp\left(-\frac{U(x)}{D}\right) \tag{25}$$

Substituting Equation (25) into Equation (17), we obtain

$$V(x) = \frac{\Theta}{D}\int \exp\left(\frac{U(x)}{D}\right)dx \tag{26}$$

In turn, we can introduce

$$\rho(x) = \left[\frac{\Theta}{D}\int \exp\left(\frac{U(x)}{D}\right)dx\right]\exp\left(-\frac{U(x)}{D}\right) \tag{27}$$

and set

$$\rho(x,t) = N(t)\exp\left(-\frac{U(x)}{D}\right) \tag{28}$$

Then, the steady-state flow intensity Θ can be expressed as

$$\Theta = \frac{DN(t)}{\int_{\sqrt{\frac{a}{b}}}^{A}\exp\left(\frac{U(x)}{D}\right)dx} \tag{29}$$

The total probability of being in the interval $(-\infty, A)$ at moment t is

$$P(t) = \int_{-\infty}^{A}\rho(x,t)dx = N(t)\int_{-\infty}^{A}\exp\left(-\frac{U(x)}{D}\right)dx \tag{30}$$

Since Θ is the rate flow with probability out of this region, at a steady state, combining Equation (29) yields

$$\frac{dP(t)}{dt} = \Theta = \frac{DN(t)}{\int_{\sqrt{\frac{a}{b}}}^{A}\exp\left(\frac{U(x)}{D}\right)dx} = \frac{DP(t)}{\int_{-\infty}^{A}\exp\left(-\frac{U(x)}{D}\right)dx\int_{-\infty}^{A}\exp\left(\frac{U(x)}{D}\right)dx} \tag{31}$$

$$P(t) = P(0)\exp(-Rt) = \exp(-Rt) \tag{32}$$

In Equation (32),

$$R^{-1} = \frac{1}{D}\int_{-\infty}^{A}\exp\left(-\frac{U(x)}{D}\right)dx\int_{-\infty}^{A}\exp\left(\frac{U(x)}{D}\right)dx \tag{33}$$

R is the Kramers escape rate, the rate at which the reaction probability flows into the unstable region. Substituting Equation (12) into Equation (33) yields the probabilistic jump rate of the non-saturated stochastic resonance between the two potential wells:

$$\begin{aligned} R_{UBSR-}^{-1} = \tfrac{1}{D}\left\{\int_{-c}^{-\sqrt{\frac{a}{b}}} \exp\left[-\tfrac{1}{D}\left(\tfrac{a^2}{4b}\left(\tfrac{x+c}{c-\sqrt{a/b}}\right)\right)\right]dx\right\} \\ \times\left\{\int_{-\sqrt{\frac{a}{b}}}^{0} \exp\left[\tfrac{1}{D}\left(-\tfrac{1}{2}ax^2+\tfrac{1}{4}bx^4\right)\right]dx\right\} \end{aligned} \tag{34}$$

Since the above equation contains the transcendental function, it is not possible to compute the exact analytical solution, so Equation (34) is solved approximately with the help of Taylor expansion by taking the constant term of the expansion equation while considering the adiabatic approximation condition constraints, i.e., $D \ll 1$. The Kramers escape rate can be approximated as

$$R_{UBSR-}^{-1} \approx \frac{4b\sqrt{a/b}\,(c-\sqrt{a/b}\,)}{a^2}\exp\left(\frac{a^2}{4bD}\right) \tag{35}$$

The same reasoning leads to

$$\begin{aligned} R_{UBSR+}^{-1} = \tfrac{1}{D}\left\{\int_{0}^{\sqrt{\frac{a}{b}}} \exp\left[-\tfrac{1}{D}\left(-\tfrac{1}{2}ax^2+\tfrac{1}{4}bx^4\right)\right]dx\right\} \\ \times\left\{\int_{\sqrt{a/b}}^{c} \exp\left[\tfrac{1}{D}\left(\tfrac{a^2}{4b}\left(\tfrac{x-c}{c-\sqrt{a/b}}\right)\right)\right]dx\right\} \end{aligned} \tag{36}$$

The Taylor expansion approximation yields

$$R_{UBSR+}^{-1} \approx \frac{4b\sqrt{a/b}\,(c-\sqrt{a/b}\,)}{a^2}\exp\left(\frac{a^2}{4bD}\right) \tag{37}$$

This yields a Kramers escape rate for the non-saturated stochastic resonance algorithm as

$$R_{UBSR} = \frac{a^2}{4b\sqrt{a/b}\,(c-\sqrt{a/b}\,)}\exp\left(-\frac{a^2}{4bD}\right) \tag{38}$$

The output signal-to-noise ratio of the bistable stochastic resonance algorithm can be expressed as

$$SNR = \pi(Ax_m/D)^2R/2 \tag{39}$$

where x_m is the potential well stabilization point and R is the Kramers escape rate.

In the unsaturated stochastic resonance algorithm, $x_m = \sqrt{a/b}$, with Equation (38) substituted into Equation (39), is obtained:

$$SNR_{UBSR} = \frac{\pi a^3A^2}{4D^2b^2\sqrt{a/b}\,(c-\sqrt{a/b}\,)}\exp\left(-\frac{a^2}{4Db}\right) \tag{40}$$

The classical stochastic resonance algorithm, $x_m = \sqrt{a/b}$, $R_{SR} = \frac{a^2}{\sqrt{2}\pi}\exp\left(-\frac{a^2}{4bD}\right)$, substituting into Equation (39), yields

$$SNR_{SR} = \frac{\sqrt{2}a^2A^2}{4D^2b^2}\exp\left(-\frac{a^2}{4Db}\right) \tag{41}$$

3.2. Accelerated Stochastic Resonance Model

It can be seen from the analysis of Figure 7 in Section 2.1 that the larger the slope of the inner measured potential well wall of the bistable system, i.e., the part of $x < |x_m|$, the more it promotes the oscillation of the particles between the potential wells. The principle is as follows: in the part of $x < |x_m|$, the slope of the potential well increases, so that the positive acceleration of the system increases and the change of the rate state of the system is obvious; in the part of $|x_m| < x < |c|$, the average slope of the potential well increases, so that the negative acceleration of the particles increases and accelerates the convergence of the system.

Combining the non-saturated stochastic resonance model proposed in Section 2.1, keeping the external potential linear, and setting the inner potential as exponential can enhance the slope of the internal potential and promote the system to leapfrog between the potential wells, while taking into account the advantages of the unsaturated output, to obtain the accelerated stochastic resonance model, which has the following potential function.

$$U_{ASR}(x) = \begin{cases} -\frac{a^2}{4b}\left(\frac{x+c}{c-\sqrt{a/b}}\right) & x < -c \\ -\frac{a^2}{4b}\left[\frac{\exp(x+c)-1}{\exp\left(c-\sqrt{a/b}\right)-1}\right] & -c \le x \le -\sqrt{a/b} \\ -\frac{a^2}{4b}\left[\frac{\exp(-x)-1}{\exp\left(\sqrt{a/b}\right)-1}\right] & -\sqrt{a/b} < x < 0 \\ -\frac{a^2}{4b}\left[\frac{\exp(x)-1}{\exp\left(\sqrt{a/b}\right)-1}\right] & 0 \le x \le \sqrt{a/b} \\ -\frac{a^2}{4b}\left[\frac{\exp(-x+c)-1}{\exp\left(c-\sqrt{a/b}\right)-1}\right] & \sqrt{a/b} < x < c \\ \frac{a^2}{4b}\left(\frac{x-c}{c-\sqrt{a/b}}\right) & x \ge c \end{cases} \quad (42)$$

A comparison of the potential function curves of the accelerated stochastic resonance system with those of the classical stochastic resonance system when the system parameters are accelerated is shown in Figure 8.

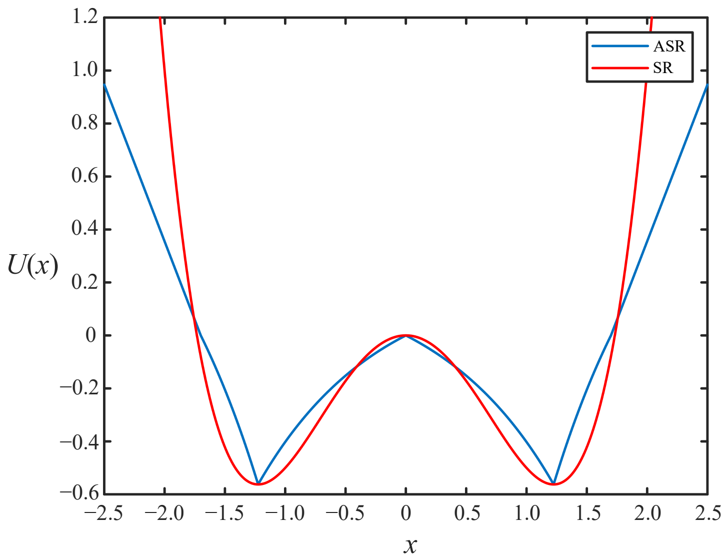

Figure 8. Accelerated stochastic resonance vs. classical stochastic resonance potential curves.

As can be seen in Figure 8, the red dashed line is the original double potential well curve, and the blue curve is the accelerated stochastic resonance potential well curve. By comparison, we can conclude that the potential function curve of accelerated stochastic resonance possesses a steeper trap wall in the inner potential well part, which can promote the oscillatory leap of particles between the two potential wells because the stochastic resonance phenomenon mainly occurs in the range of $x \le |c|$, while the peripheral potential well wall maintains the linear characteristics of the non-saturating stochastic resonance, so the amplitude of the output signal of the system no longer tends to a stable saturation value at time $t \to \infty$, and instead, it increases linearly, avoiding the output saturation phenomenon.

Disregarding the effect of noise, when the signal of Equation (13) is input to the system, the system potential function is modulated by the input signal, and the potential function curve is shown in Figure 9.

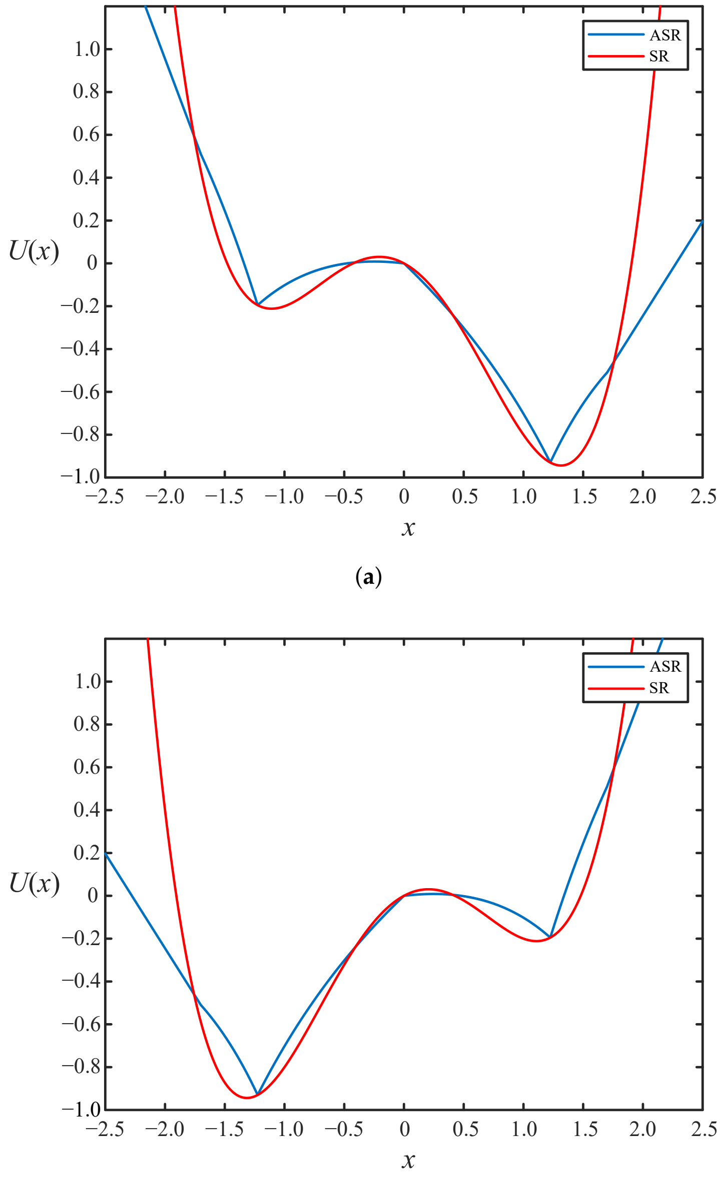

Figure 9. Potential function curves under input signal modulation. (**a**) Potential function curves at quarter-cycle moments. (**b**) Potential function curve at the moment of three-quarter cycle.

As can be seen in Figure 9, the depth of the left and right potential wells of the accelerated stochastic resonance potential function undergoes alternating transformations, and the period of its dynamic change is consistent with the period of the signal to be detected. The slope of the internal potential function of the accelerated stochastic resonance detection system is always larger than that of the original stochastic resonance signal detection algorithm, indicating that it can promote the oscillation of the particles between the two potential wells, reduce the energy loss, and improve the conversion rate of the noise energy to the signal energy.

This is obtained by substituting $U_{ASR}(x)$ into Equation (33) and solving for the approximate solution:

$$R_{ASR} \approx \frac{D}{\sqrt{a/b}\,(c-\sqrt{a/b}\,)} \exp\left[-\frac{a^2(\exp(c)-1)}{4Db(\exp(c-\sqrt{a/b}\,)-1)}\right] \tag{43}$$

Substituting Equation (43) into Equation (39) yields the output signal-to-noise ratio of the accelerated stochastic resonance system:

$$SNR_{ASR} = \frac{\pi a A^2}{2Db\sqrt{a/b}\,(c-\sqrt{a/b}\,)} \exp\left[-\frac{a^2(\exp(c)-1)}{4Db(\exp(c-\sqrt{a/b}\,)-1)}\right] \tag{44}$$

Setting the system parameters $a = 1.5$, $b = 1$, and the input signal amplitude A = 0.35, the relationship curves of the signal-to-noise ratios of Equations (40), (41) and (44) plotted as a function of the variation of the input noise intensity D are shown in Figure 10.

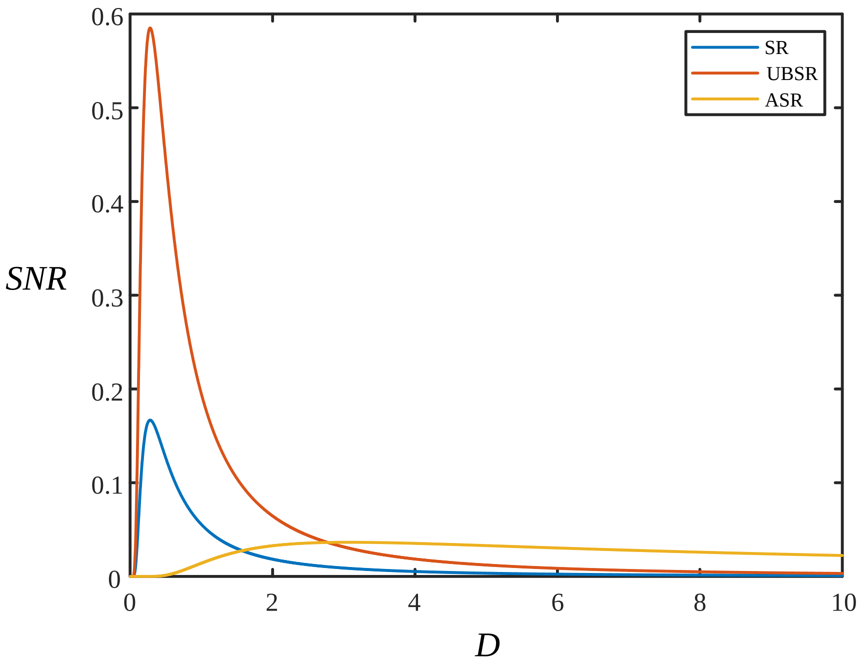

Figure 10. Output SNR versus noise intensity D.

As can be seen from Figure 10, the output SNR of the unsaturated stochastic resonance algorithm is always higher than that of the classical stochastic resonance algorithm, while the output SNR of the proposed accelerated stochastic resonance algorithm is better than that of the unsaturated stochastic resonance algorithm and the classical stochastic resonance algorithm when the noise intensity D is larger than 2.8, which shows that the accelerated stochastic resonance algorithm has a significant advantage in larger noise intensities, and this is because of the exponentially shaped inner potential well walls promote the particle. The reason is that the exponential inner potential well wall promotes the jumping process between the potential wells.

It is verified through simulation that the amplitude A of the input signal only affects the height of the output signal-to-noise ratio curve and does not affect the curve trend distribution so that the system with the same parameters has the same response curve to the noise intensity.

4. Case Simulation and Result Analysis

4.1. Harmonic Signal Detection Experiment

The power system's harmonic simulation signal from the study [20] is used for simulation, and the target harmonic signal is

$$s(t) = A_1 \sin(2\pi f_1 t) + A_2 \sin(2\pi f_2 t) + A_3 \sin(2\pi f_3 t) + A_4 \sin(2\pi f_4 t) + A_5 \sin(2\pi f_5 t) \quad (45)$$

Which $A_1 = 1$, $A_2 = 0.15$, $A_3 = 0.25$, $A_4 = 0.2$, $A_5 = 0.1$, $f_0 = 50$ Hz, $f_1 = f_0$, $f_2 = 2.2f_0$, $f_3 = 3f_0$, $f_4 = 5f_0$, $f_5 = 7f_0$.

For easy understanding, in the simulation experiments of this paper, $s(t)$ values all denote the ideal target signal contained in the noise-containing signal of the input stochastic resonance system, $n(t)$ values all denote the random noise contained in the noise-containing signal of the input stochastic resonance system, $S(f)$ values denote the amplitude–frequency spectral value of the ideal target signal, and $N(f)$ values denote the amplitude–frequency spectral value of the random noise. $x(t)$ denotes the output signal of the stochastic resonance detection system, which is essentially a time course of the characteristic displacements of the bistable system, and $X(f)$ is the amplitude–frequency spectral value of the output signal of the stochastic resonance system. which is essentially the time course of the characteristic displacements of the bistable system, and $X(f)$ is the amplitude–frequency spectral value of the output signal of the stochastic resonance system.

Setting the system parameters as $a = 1.5$, $b = 1$, $c = 2$, Gaussian white noise with noise intensity D of 1 is mixed with the harmonic signals of Equation (45) through the secondary sampling process [21] and inputted to the classical stochastic resonance detection system, the unsaturated stochastic resonance detection system, and the accelerated stochastic resonance detection system, and the fourth-order Runge–Kutta algorithm is utilized for the calculation of Langevin equation [22]. The mixed signal waveforms and spectra are shown in Figure 11, and the experimental results are shown in Figures 12–14.

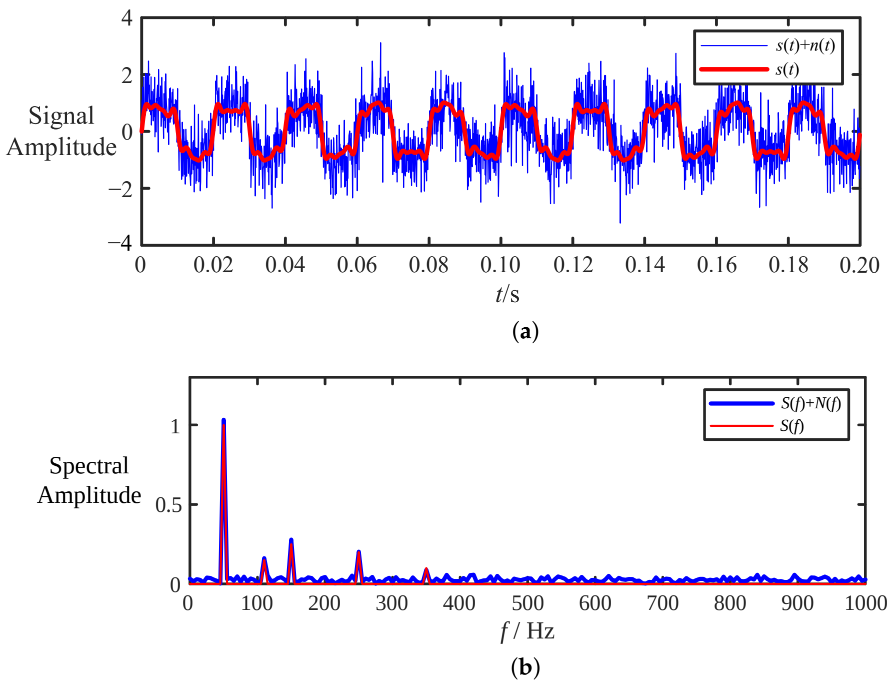

Figure 11. Input noise signal waveform and spectrum at D = 1. (**a**) Time domain waveform. (**b**) Spectral amplitude.

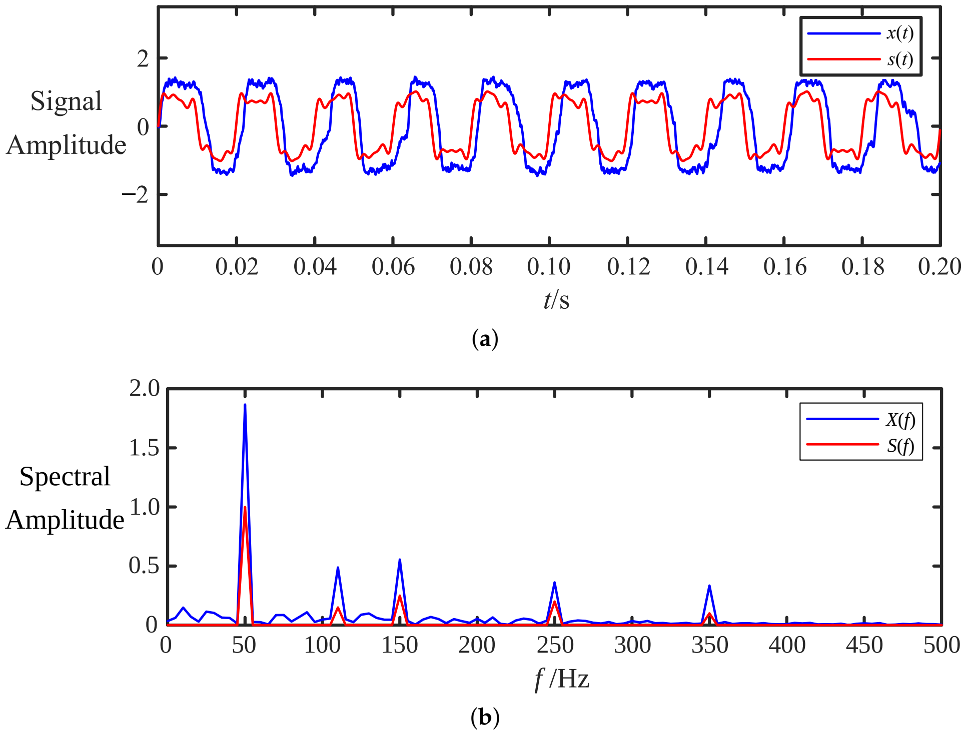

Figure 12. SR detection system output signal waveform and spectrum at $D = 1$. (**a**) Time domain waveform. (**b**) Spectral amplitude.

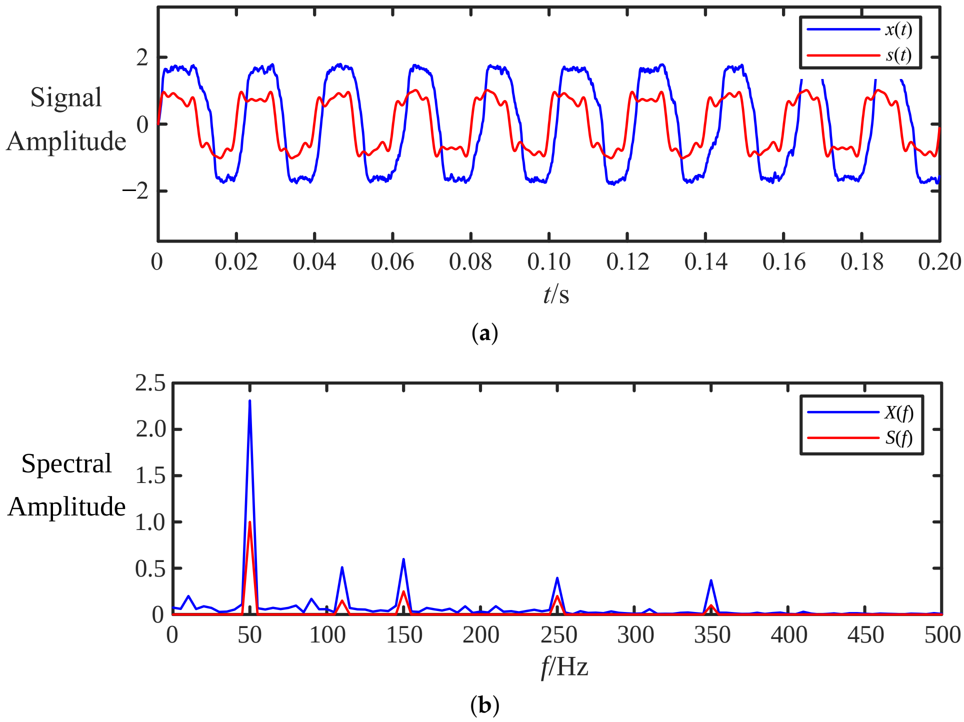

Figure 13. UBSR detection system output signal waveform and spectrum at $D = 1$. (**a**) Time domain waveform. (**b**) Spectral amplitude.

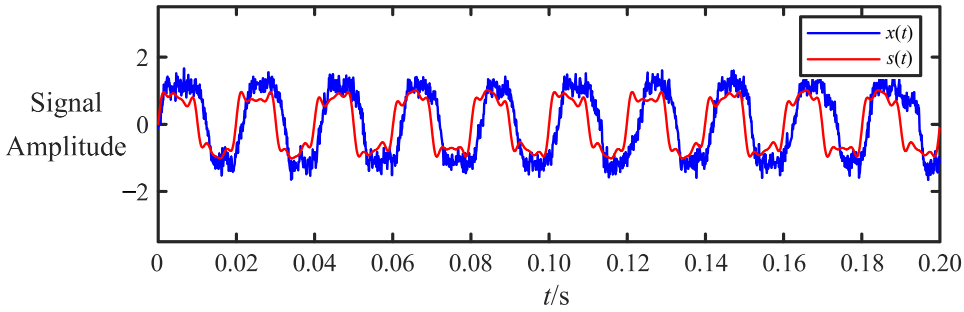

(**a**)

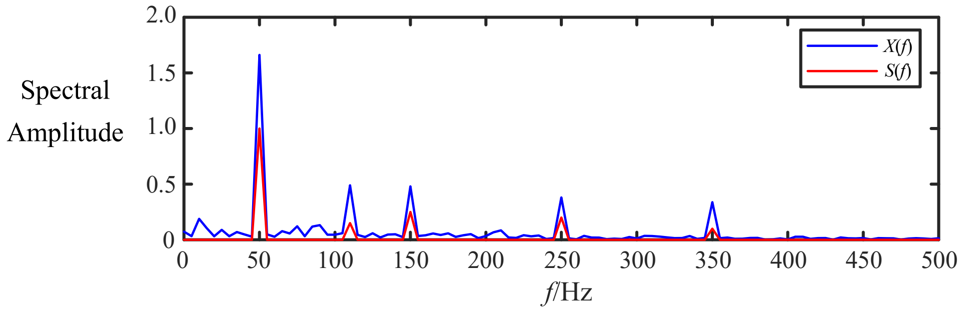

(**b**)

Figure 14. ASR detection system output signal waveform and spectrum at D = 1. (**a**) Time domain waveform. (**b**) Spectral amplitude.

Comparing Figure 11 with Figures 12–14, it can be seen that all three stochastic resonance detection models can realize the conversion of noise energy to signal energy, which in turn suppresses the noise and improves the signal-to-noise ratio. Comparing the output signals of Figures 12–14, it can be seen that under the low-intensity noise interference, the non-saturated stochastic resonance improves the amplitude of the output of the system and has the highest output signal-to-noise ratio, the classical stochastic resonance system has an intermediate output signal-to-noise ratio, and the accelerated stochastic resonance system has the lowest output signal-to-noise ratio, which is in line with the conclusions of the previous derivation.

The Gaussian white noise with a noise intensity D of 5 is mixed with the harmonic signals of Equation (45) through the secondary sampling process and then input to the classical stochastic resonance detection system, unsaturated stochastic resonance detection system, and accelerated stochastic resonance detection system, and the subsequent signals are all processed by the secondary sampling process, and the fourth-order Runge–Kutta algorithm is used to calculate the Langevin equations. The waveforms and spectra of the mixed signals are shown in Figure 15, and the experiment results are shown in Figures 16–18. The results are shown in Figures 16–18.

Comparing Figure 15 with Figures 16–18, it can be seen that the classical stochastic resonance detection system and the unsaturated stochastic resonance detection system do not have a stochastic resonance phenomenon under strong noise interference, and only the accelerated stochastic resonance detection system realizes the conversion of the noise energy to the signal energy, suppresses the noise, and succeeds in having stochastic resonance. The results of this experiment also show that the steeper internal potential well wall can effectively promote the oscillatory jump of particles between potential wells, which is consistent with the previous derivation.

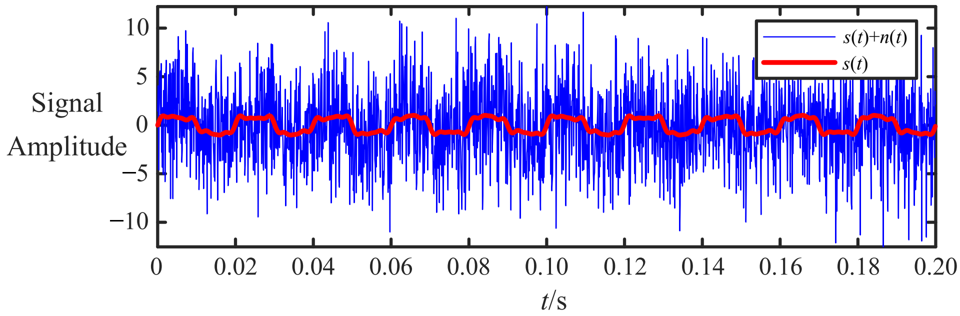

(**a**)

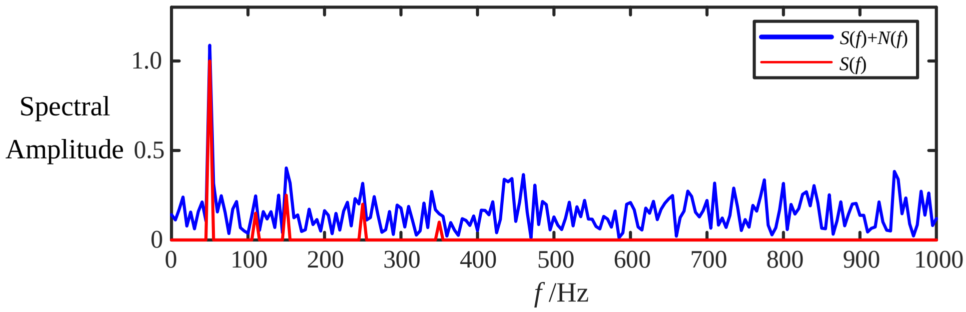

(**b**)

Figure 15. Input Noise signal waveform and spectrum at D = 5. (**a**) Time domain waveform. (**b**) Spectral amplitude.

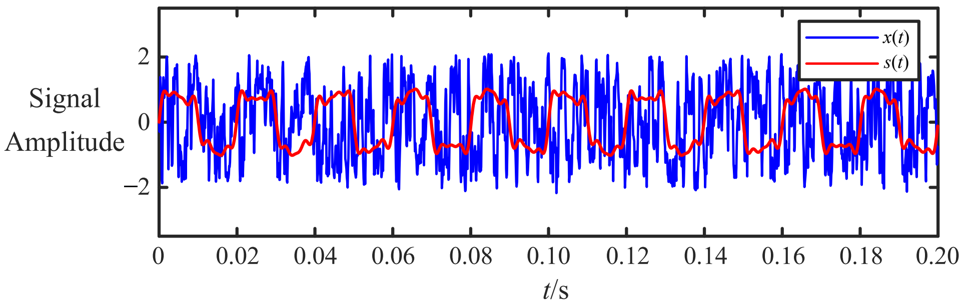

(**a**)

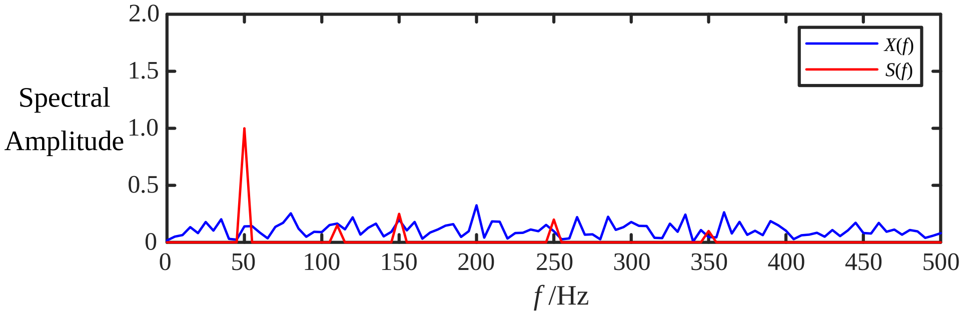

(**b**)

Figure 16. SR detection system output signal waveform and spectrum at D = 5. (**a**) Time domain waveform. (**b**) Spectral amplitude.

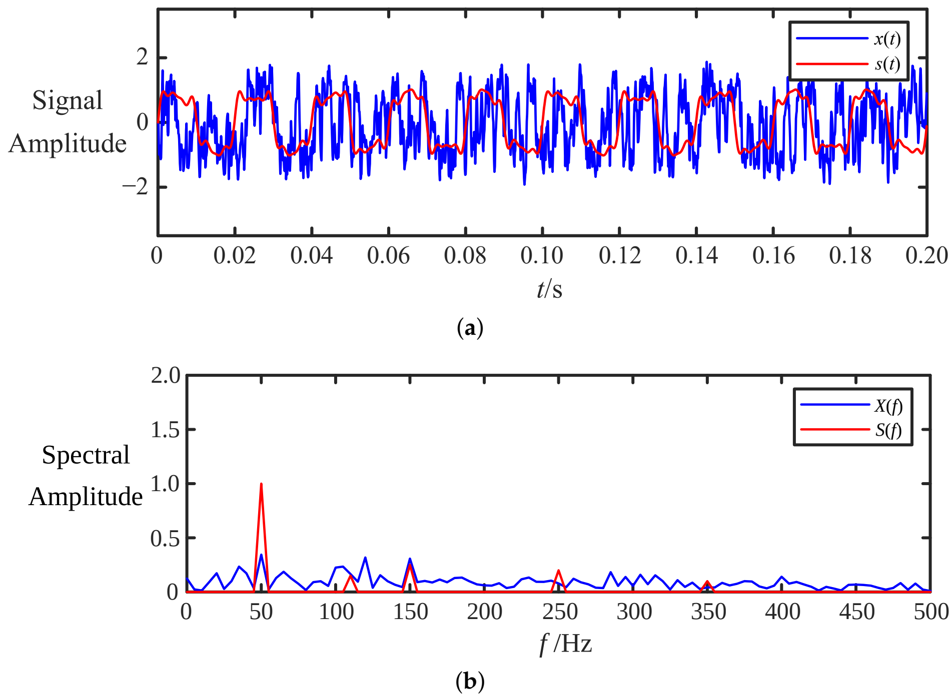

Figure 17. UBSR detection system output signal waveform and spectrum at D = 5. (**a**) Time domain waveform. (**b**) Spectral amplitude.

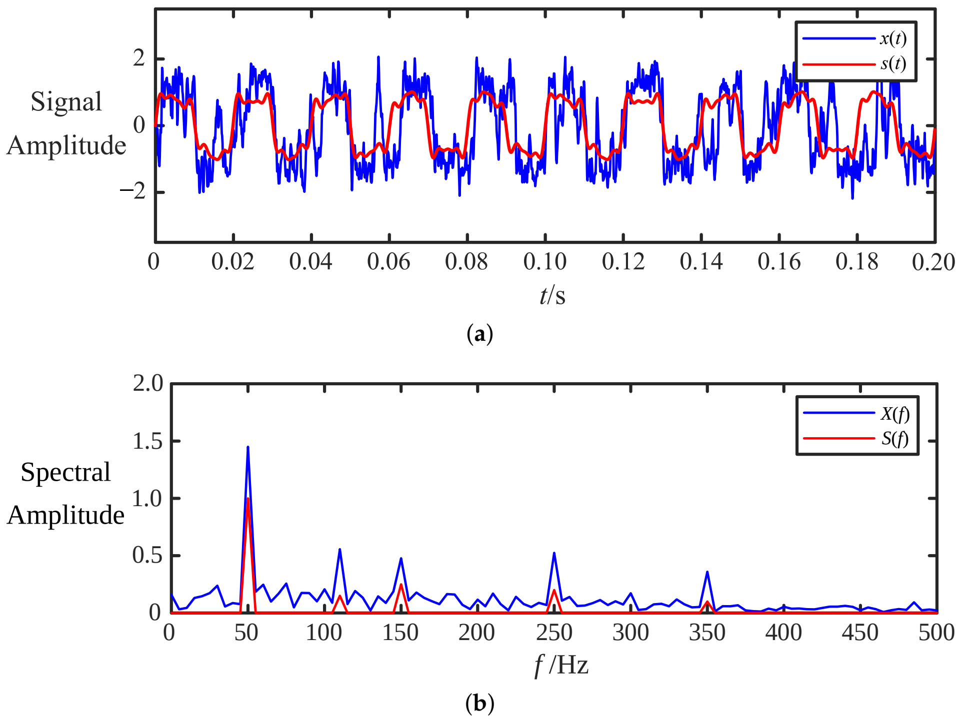

Figure 18. ASR detection system output signal waveform and spectrum at D = 5. (**a**) Time domain waveform. (**b**) Spectral amplitude.

The detection accuracies of the three stochastic resonance detection methods were analyzed to determine the frequency of each harmonic component based on the spectrum, as shown in Table 1.

Table 1. Harmonic frequency detection results of three stochastic resonance systems. (a) $D = 1$. (b) $D = 5$.

	f/Hz	**SR**	**UBSR**	**ASR**
(a) $D = 1$	50	50	50	50
	110	110	110	110
	150	150	150	150
	250	250	250	250
	350	350	350	350
(b) $D = 5$	50	50	50	50
	110	110	110	110
	150	150	150	150
	250	250	250	250
	350	350	350	350

As can be seen from Table 1, all three stochastic resonance detection systems are able to realize the difference-free detection of harmonic frequencies under the interference of weak and strong noises, which depends on the fact that the stochastic resonance system driven by the periodic signal will not affect the frequency of the driving signal but instead clamps the random noise to oscillate the output at the driving frequency, which is a unique advantage of the stochastic resonance detection principle relative to the traditional detection methods.

4.2. Voltage Transient Droop Signal Detection Experiment

In order to verify the applicability of the accelerated stochastic resonance for other categories of power system periodic characteristic signals in strong noise environments, the voltage-dropout signal is used as the simulated fault signal, and the input simulated fault signal is

$$s(t) = (1 - v(u(t_2) - u(t_1)))\sin(2\pi f_0 t) \tag{46}$$

In the formula, $v = 0.8$; $f_0 = 50$ Hz; $u(t_1)$ and $u(t_2)$ are the step signals generating sudden changes at the moments of t_1 and t_2, respectively; $t_1 = 0.13$; and $t_2 = 0.07$. Gaussian white noise $n(t)$ with a noise intensity D of 1 is mixed in, the sampling frequency is $f_s = 2000$ Hz, and the number of sampling points is $L = 5000$, so as to obtain the noise-containing voltage-dropout fault signal. Setting the system parameters $a = 1.5$, $b = 1$, $c = 2$, the fourth-order Runge–Kutta algorithm is utilized to calculate the Langevin equation, the waveforms and spectra of the voltage-dropout signals are shown in Figure 19, and the experimental results are shown in Figures 20–22.

The purpose of the detection of the voltage transient signal is to determine the voltage transient and voltage recovery moments, so the output signal-to-noise ratio cannot be used as a separate evaluation index to measure the performance of the algorithm [23]; therefore, the number of interrelationships between the input and output signals is introduced as an evaluation index, which is used to measure the phase-matching relationship between the output signal of the stochastic resonance and the original input signal, and the number of interrelationships between input and output signals ρ_{SX} expression is as follows:

$$\begin{cases} R_{SX}(\tau) = \int_{-\infty}^{+\infty} [s(t) + n(t)] \cdot x(t+\tau)dt \\ \rho_{SX} = \frac{R_{SX}(\tau)}{\sqrt{R_S(0) \cdot R_X(0)}} \end{cases} \tag{47}$$

where R_S and R_X are the autocorrelation coefficients of the input and output signals of the stochastic resonance system, respectively.

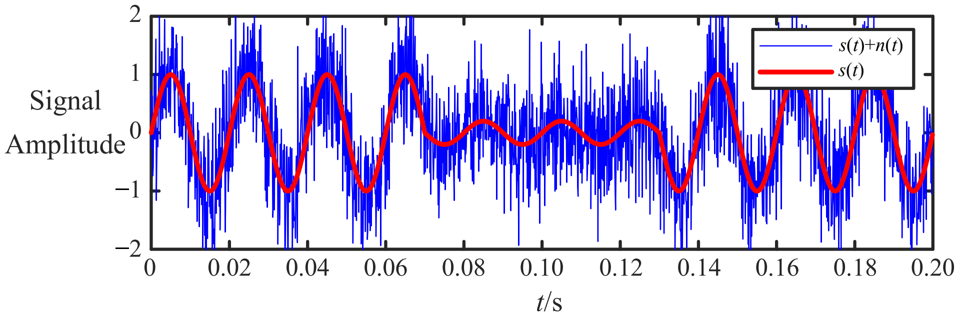

(**a**)

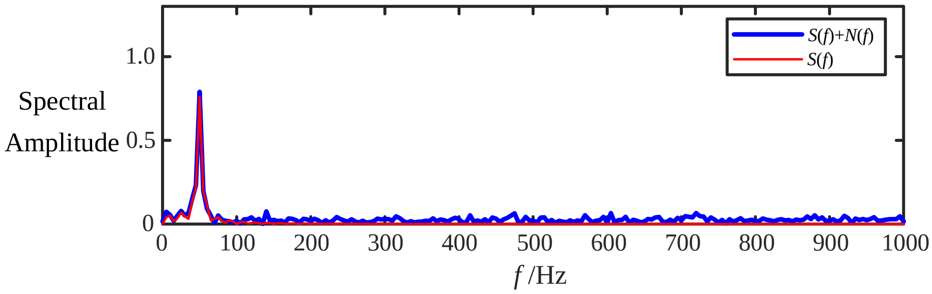

(**b**)

Figure 19. Input noise-containing voltage drop signal waveform and spectrum at D = 1. (**a**) Time domain waveform. (**b**) Spectral amplitude.

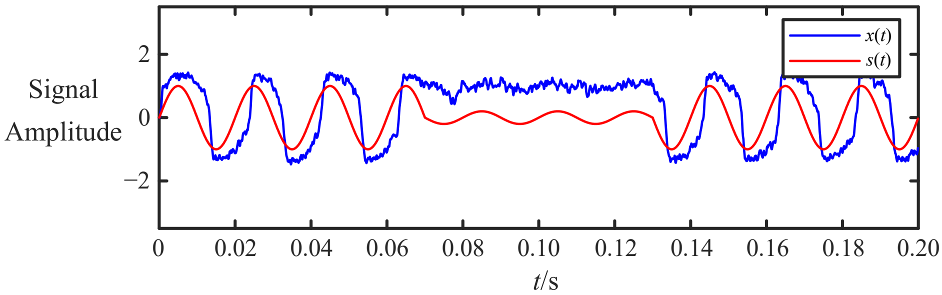

(**a**)

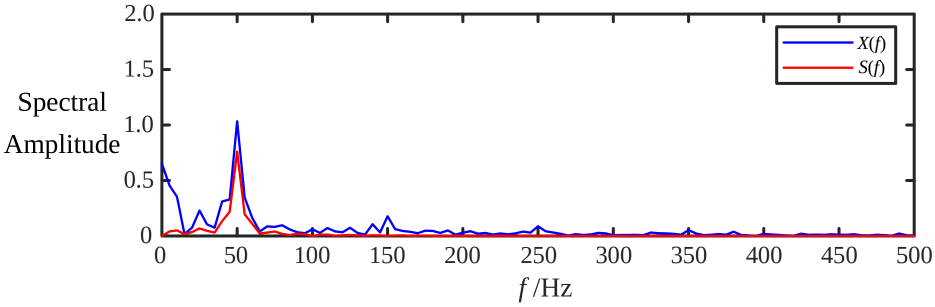

(**b**)

Figure 20. SR detection system output signal waveform and spectrum at D = 1. (**a**) Time domain waveform. (**b**) Spectral amplitude.

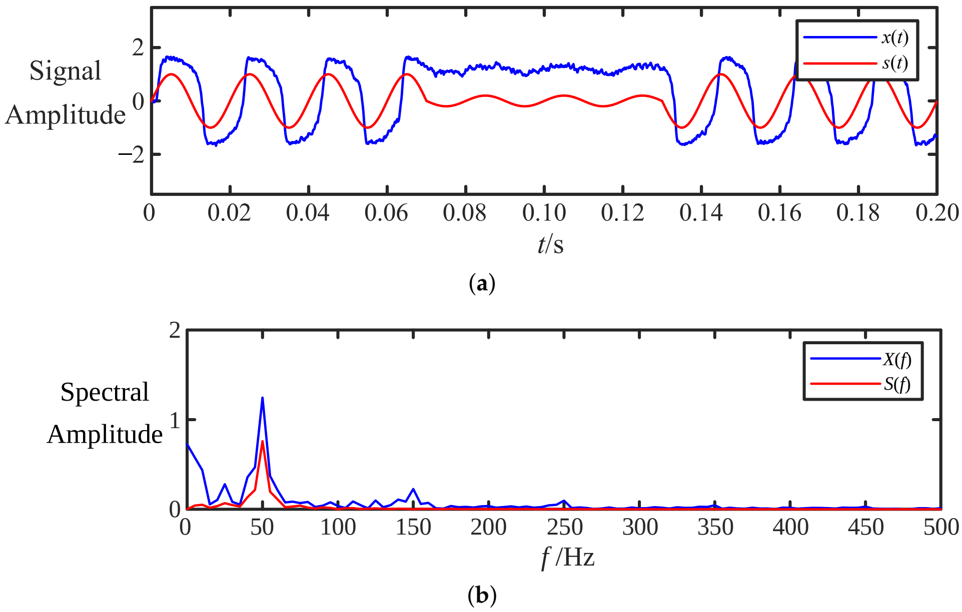

Figure 21. UBSR detection system output signal waveform and spectrum at D = 1. (**a**) Time domain waveform. (**b**) Spectral amplitude.

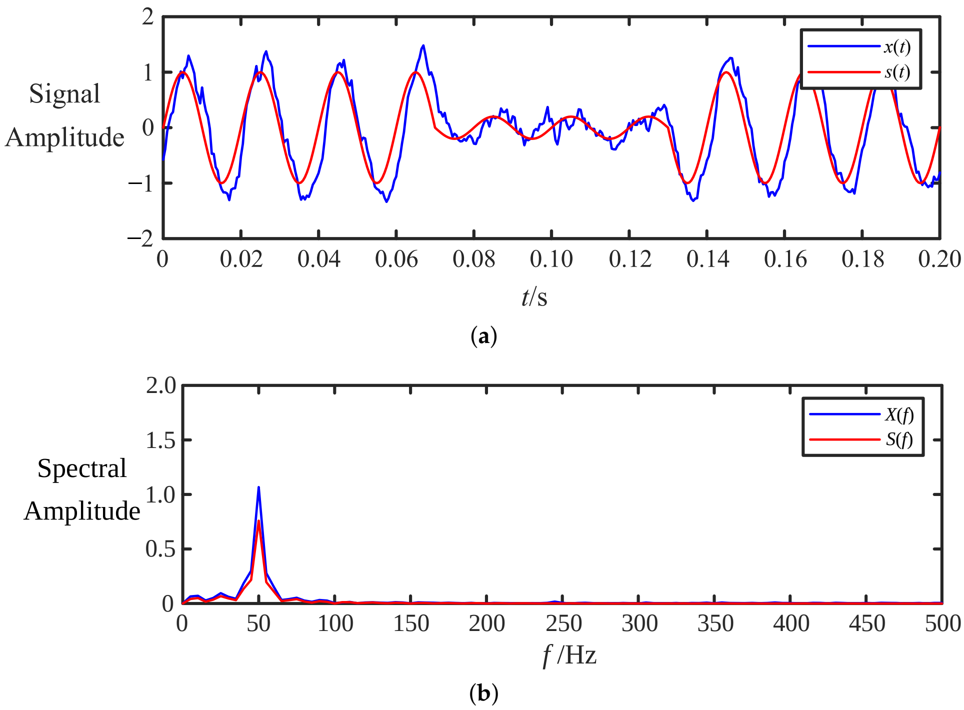

Figure 22. ASR detection system output signal waveform and spectrum at D = 1. (**a**) Time domain waveform. (**b**) Spectral amplitude.

Comparing Figure 19 with Figures 20–22, it can be seen that all three stochastic resonance detection models can realize the conversion of noise energy to signal energy, which in turn suppresses the noise and improves the signal-to-noise ratio. Comparing the output signals of Figures 20–22, it can be seen that under low-intensity noise interference, the non-saturated stochastic resonance improves the amplitude of the system output and has the highest output signal-to-noise ratio, while the classical stochastic resonance system has the middle output signal-to-noise ratio, and the accelerated stochastic resonance system has the lowest output signal-to-noise ratio, which is in line with the conclusions of the previous derivation. However, the output signals of the classical stochastic resonance detection system and the unsaturated stochastic resonance detection system have more obvious waveform distortion in the part of the voltage transient, mainly due to the fact that the voltage transient will make the sinusoidal signal appear harmonics, but the harmonics are relatively very weak, and in the presence of the 50 Hz voltage signal, it cannot affect the shape of the potential well. In the presence of the noise, the harmonic energy is clamped by the noise energy, which is partially transformed into low-frequency energy of random noise, which is evident in the spectrum of the output signal. The accelerated stochastic resonance detection system, due to the larger slope of the potential well wall in the exponential type, makes the displacement span of the particle jumping in the trap smaller, which equivalently weakens the control effect of the random noise on the particle state in the process of jumping, and the waveform distortion of the system is smaller at this time, which also reflects the unique advantages of the accelerated stochastic resonance detection system.

The Gaussian white noise $n(t)$ with a noise intensity D of 5 is mixed in, the system parameters $a = 1.5$, $b = 1$, $c = 2$ are set, and the fourth-order Runge–Kutta algorithm is utilized for the calculation of the Langevin equation. The voltage transient drop signal waveforms and spectra are shown in Figure 23, and the experimental results are shown in Figures 24–26.

Comparing Figure 23 with Figures 24–26, it can be seen that the classical stochastic resonance detection system has no stochastic resonance phenomenon under strong noise interference, the degree of stochastic resonance of the non-saturated stochastic resonance detection system is weaker, and only the accelerated stochastic resonance detection system succeeds in the occurrence of stochastic resonance, which realizes the transformation of the noise energy to the signal energy, suppresses the noise, and improves the signal-to-noise ratio, and the signal main frequency of 50 Hz error-free detection was realized. Meanwhile, the output signals of the classical stochastic resonance detection system and the non-saturated stochastic resonance detection system have waveform distortion in the voltage transient part, as in the case of weak noise interference.

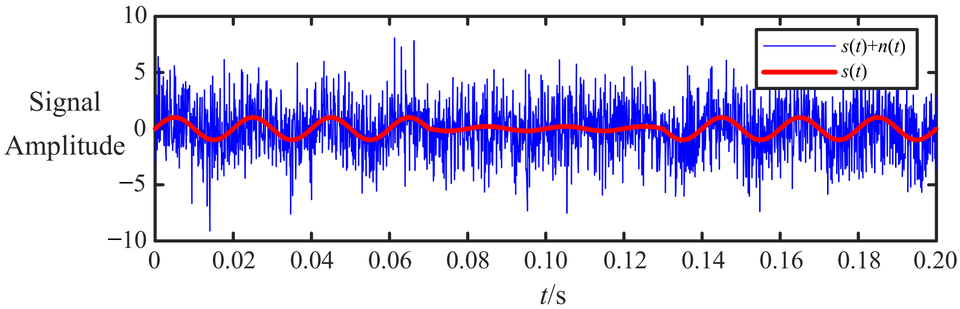

(**a**)

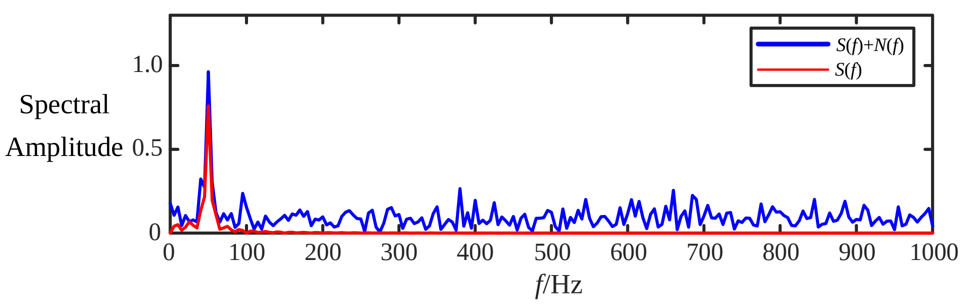

(**b**)

Figure 23. Input noise-containing voltage drop signal waveform and spectrum at D = 5. (**a**) Time domain waveform. (**b**) Spectral amplitude.

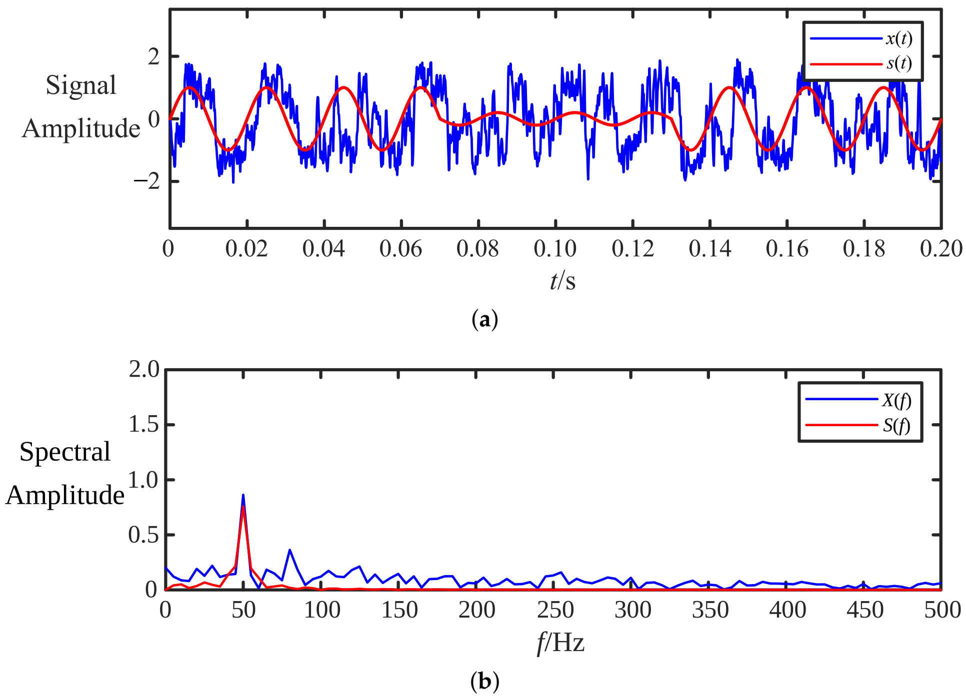

Figure 24. SR detection system output signal waveform and spectrum at $D = 5$. (**a**) Time domain waveform. (**b**) Spectral amplitude.

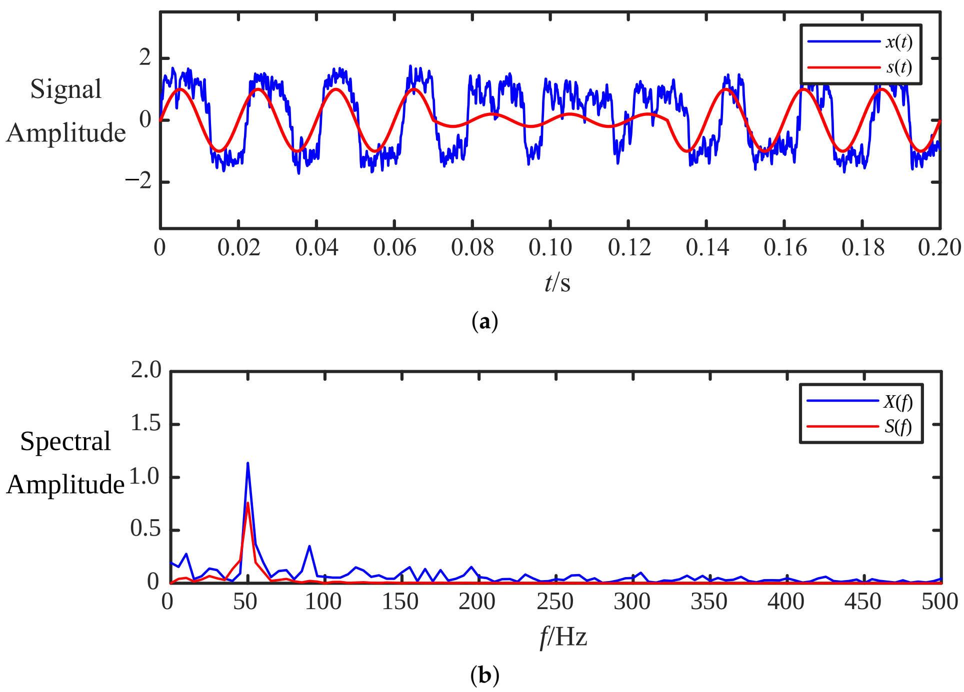

Figure 25. UBSR detection system output signal waveform and spectrum at $D = 5$. (**a**) Time domain waveform. (**b**) Spectral amplitude.

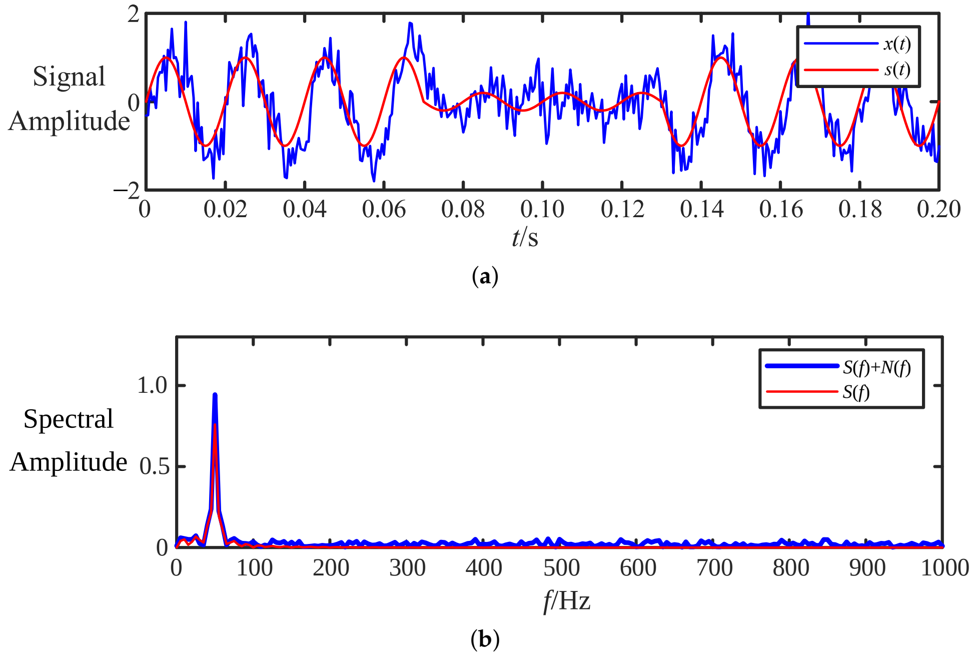

Figure 26. ASR detection system output signal waveform and spectrum at D = 5. (**a**) Time domain waveform. (**b**) Spectral amplitude.

In order to better measure the accuracy of different stochastic resonance systems in detecting the moment of voltage transient drop, as well as the moment of voltage return, the number of interrelationships between the input and output signals of each stochastic resonance detection system is calculated, and the results are shown in Table 2.

Table 2. Number of correlations between the input and output signals of various stochastic resonance detection systems.

	$D = 1$	$D = 5$
SR	0.6132	0.1743
UBSR	0.6439	0.3972
ASR	0.9879	0.9794

As can be seen from Table 2, only the accelerated stochastic resonance detection system can better maintain the signal phase and waveform, which can reduce the distortion of the classical stochastic resonance detection system. Although the output signal-to-noise ratio of ASR is lower than that of SR and UBSR in the case of weak noise disturbances, the unique noise immunity and the anti-distortion capability are highlighted in the case of strong noise disturbances.

4.3. Comparison of Method Computational Efficiency

Taking the voltage transient signal detection experiment as an example, the computing time consumption of the three stochastic resonance detection systems is recorded, and the detection real-time comparison is made with the plus-window interpolation FFT, VMD, EEMD, and empirical wavelet transform methods, and the results are shown in Table 3.

Table 3. Comparison of real-time performance of different detection methods.

Methodologies	Plus Window Interpolation FFT	VMD	EEMD	Empirical Wavelet Tranform	SR	UBSR	ASR
time-consuming/s	1.032	2.3814	7.5216	2.0105	0.8123	1.0117	1.2361

As can be seen from Table 3, the classical stochastic resonance detection algorithm has a lower computational amount compared to the traditional methods such as time-frequency domain detection and has good real-time detection. Additionally non-saturated stochastic resonance detection methods and accelerated stochastic resonance detection methods, relative to the classical stochastic resonance detection methods, just slightly increase the amount of computation, and they still have a higher arithmetic efficiency.

5. Conclusions

The classic bistable stochastic resonance algorithm has inherent output saturation defects. This paper introduces a non-saturated bistable stochastic resonance signal detection algorithm and an accelerated stochastic resonance signal detection algorithm based on the segmented potential function to address this issue. The output signal of the classic algorithm is limited by the quadratic term in its potential function, which impacts the detection performance. To overcome this limitation, the proposed algorithms are based on the segmented potential function without higher-order terms, optimizing the algorithm structure. The paper also derives the Kramers escape rate and output signal-to-noise ratio expressions of the algorithms theoretically to ensure their feasibility. Simulation experiments demonstrate that the proposed algorithm exhibits better weak-signal enhancement capability and faster detection speed compared to the classic bistable stochastic resonance algorithm. Furthermore, it significantly improves the detection accuracy of power system harmonics and various types of periodic characteristic signals compared to traditional time-frequency domain detection methods.

In future research, the single-trap approximation model for unsaturated stochastic resonance detection system and accelerated stochastic resonance detection system is investigated, and the model performance of the single traps of UBSR, as well as ASR, is analyzed with reference to the stochastic resonance single-trap approximation model proposed by us in the literature [20], which extends the detection object to non-periodic signals.

Author Contributions: Conceptualization, S.S. and X.Q.; methodology, X.Q.; software, X.Q.; validation, Z.Y. and Z.L.; formal analysis, Z.Y.; investigation, X.T.; resources, X.T. and Z.L.; data curation, Z.Y. and X.T.; writing—original draft preparation, X.Q., S.S., and Z.Y.; writing—review and editing, X.Q., S.S. and Z.L.; visualization, X.Q. and S.S.; supervision X.T. and Z.L.; project administration, S.S.; funding acquisition S.S. All authors have read and agreed to the published version of the manuscript.

Funding: This work was supported in part by the National Natural Science Foundation of China: A Novel Power System Inertia Power Frequency Multi spatiotemporal Coupling Mechanism and Wide Area Coordinated Control (U22B20109); State Grid Corporation Science and Technology Project: Research on DC Control Optimization to Improve the Dynamic and Transient Performance of AC/DC Hybrid Power Grid (5100-202124011A-0-0-00).

Institutional Review Board Statement: Not applicable.

Informed Consent Statement: Not applicable.

Data Availability Statement: Sharing of the data used in this study is limited due to the privacy restrictions of the project. If necessary, the data can be obtained by contacting the corresponding author.

Conflicts of Interest: The authors declare no conflicts of interest.

References

1. Shu, Y.; Tang, Y. Analysis and recommendations for the adaptability of China's power system security and stability relevant standards. *CSEE J. Power Energy Syst.* **2017**, *3*, 334–339. [CrossRef]
2. Wang, Y.; Xu, J.; Xu, H.; Long, F. The Application Study of the Advanced Power Electronics in the Smart Grid. In Proceedings of the 2017 Sixth International Conference on Future Generation Communication Technologies (FGCT), Dublin, Ireland, 21–23 August 2017.
3. Li, X.; Wang, S. Energy management and operational control methods for grid battery energy storage systems. *CSEE J. Power Energy Syst.* **2021**, *7*, 1026–1040. [CrossRef]
4. Liao, K.; Pang, B.; Yang, J.; Jin, X.; Chen, B.; He, Z. Enhanced compensation strategy of voltage harmonics for Doubly-Fed induction generator. *Int. J. Electr. Power Energy Syst.* **2023**, *148*, 108924. [CrossRef]
5. Lei, H.; Huang, Y.; Jiang, L.; Gao, G.; Zhang, J.; Wu, P. Research on Fourier and Prony analysis algorithm of inter-harmonic in power system. *Energy Rep.* **2022**, *8*, 728–737. [CrossRef]
6. Shu, S.; Lai, J.; Chen, Z.; Wang, Y.; Zhang, Y.; Tao, X.; Lang, X.; Chen, J. Design and implementation of plasma electron density measurements based on FPGA with all-phase FFT for tokamak devices. *Rev. Sci. Instrum.* **2021**, *92*, 093507. [CrossRef]
7. Liu, Z.; Du, T. Anti-aliasing wavelet packet method for harmonic detection. *J. Syst. Eng. Electron.* **2009**, *20*, 197–203.
8. Ortiz-Medina, R.A.; Sanabria-Villamizar, M.; Lopez-Garcia, I.; Villalobos-Piña, F.J.; Beltran-Carbajal, F.; Maldonado-Ruelas, V.A. Wavelet and Hilbert Huang Transforms Applied to Park's Vector for Fault Detection in a PMSG Wind Turbine. In Proceedings of the 2023 IEEE 6th Colombian Conference on Automatic Control (CCAC), Papayan, Colombia, 17–20 October 2023; pp. 1–6. [CrossRef]
9. Gong, S.; Li, S.; Wang, H.; Ma, H.; Yu, T. Multi-Frequency Weak Signal Detection Based on Wavelet Transform and Parameter Selection of Bistable Stochastic Resonance Model. *J. Vib. Eng. Technol.* **2021**, *9*, 887–906. [CrossRef]
10. Xiao, F.-H.; Yan, G.-R.; Zhang, X.-W. Effect of signal modulating noise in bistable stochastic dynamical systems. *Chin. Phys.* **2003**, *12*, 946. [CrossRef]
11. Qiu, Q.; Jiang, S.; Yuan, S.; Shi, X.; Li, L.; Wang, Z.; Zhang, X.; Qin, D.; Guo, F.; Wang, L.; et al. Influence of colored cross-correlated noise on stochastic resonance for an underdamped bistable system subjected to multiplicative and additive noises. *Phys. Scr.* **2023**, *98*, 075001. [CrossRef]
12. Leng, Y.-G.; Wang, T.-Y.; Guo, Y.; Wu, Z.-Y. Study of the property of the parameters of bistable stochastic resonance. *Acta Phys. Sin.* **2007**, *56*, 30. [CrossRef]
13. Xu, Z.; Wang, Z.; Yang, J.; Sanjuán, M.A.F.; Sun, B.; Huang, S. Aperiodic stochastic resonance in a biased monostable system excited by different weak aperiodic pulse signals and strong noise. *Eur. Phys. J. Plus* **2023**, *138*, 386. [CrossRef]
14. Chew, L.Y.; Ting, C.; Lai, C.H. Chaotic resonance: Two-state model with chaos-induced escape over potential barrier. *Phys. Rev. E* **2005**, *72*, 036222. [CrossRef] [PubMed]
15. Wang, S.; Niu, P.; Guo, Y.; Wang, F.; Han, S. A Piecewise Hybrid Stochastic Resonance Method for Early Fault Detection of Roller Bearings. *IEEE Access* **2020**, *8*, 73320–73329. [CrossRef]
16. Mi, L.N.; Guo, Y.F.; Zhang, M.; Zhuo, X.J. Stochastic resonance in gene transcriptional regulatory system driven by Gaussian noise and Lévy noise. *Chaos Solitons Fractals* **2023**, *167*, 113096. [CrossRef]
17. Liu, J.; Mao, J.; Huang, B.; Liu, P. Chaos and reverse transitions in stochastic resonance. *Phys. Lett. A* **2018**, *382*, 3071–3078. [CrossRef]
18. Kim, S.; Reichl, L.E. Stochastic chaos and resonance in a bistable stochastic system. *Phys. Rev. E* **1996**, *53*, 3088–3095. [CrossRef]
19. Pankratov, A.L.; Salerno, M. Adiabatic approximation and parametric stochastic resonance in a bistable system with periodically driven barrier. *Phys. Rev. E* **2000**, *61*, 1206–1210. [CrossRef]
20. Sun, S.; Qi, X.; Yuan, Z.; Tang, X.; Li, Z. Detection of Weak Fault Signals in Power Grids Based on Single-Trap Resonance and Dissipative Chaotic Systems. *Electronics* **2023**, *12*, 3896. [CrossRef]
21. Leng, Y.g.; Lai, Z.; Fan, S.B.; Gao, Y. Large parameter stochastic resonance of two-dimensional Duffing oscillator and its application on weak signal detection. *Wuli Xuebao/Acta Phys. Sin.* **2012**, *61*, 230502. [CrossRef]
22. Ji, C.; Zhao, Q.; Yu, Y.; Dai, W. Detection of Weak Signals Under Low SNR Stochastic Resonance System. *IEEE Access* **2023**, *11*, 101881–101889. [CrossRef]
23. Kasai, S. Stochastic resonance in nanodevice parallel systems. In Proceedings of the 2009 International Symposium on Intelligent Signal Processing and Communication Systems (ISPACS), Kanazawa, Japan, 7–9 December 2009; pp. 363–366. [CrossRef]